# Dissociation dynamics of positive-ion and negative-ion fragments of gaseous and condensed Si ( C H 3 ) 2 Cl 2 via Si 2 p , Cl 2 p , and Cl 1 s core-level excitations

J. M. Chen, K. T. Lu, J. M. Lee, C. K. Chen, and S. C. Haw

Citation: The Journal of Chemical Physics **125**, 214303 (2006); doi: 10.1063/1.2400229
View online: http://dx.doi.org/10.1063/1.2400229
View Table of Contents: http://scitation.aip.org/content/aip/journal/jcp/125/21?ver=pdfcov
Published by the AIP Publishing

# Dissociation dynamics of positive-ion and negative-ion fragments of gaseous and condensed $Si(CH_3)_2Cl_2$ via Si 2*p*, Cl 2*p*, and Cl 1*s* core-level excitations

J. M. Chen[a),b)] and K. T. Lu[a)]
*National Synchrotron Radiation Research Center, Hsinchu 30076, Taiwan, Republic of China*

J. M. Lee
*National Synchrotron Radiation Research Center, Hsinchu 30076, Taiwan, Republic of China and*
*Department of Electrophysics, National Chiao Tung University, Hsinchu 30010, Taiwan Republic of China*

C. K. Chen and S. C. Haw
*National Synchrotron Radiation Research Center, Hsinchu 30076, Taiwan, Republic of China*

(Received 26 September 2006; accepted 26 October 2006; published online 1 December 2006)

The state-selective positive-ion and negative-ion dissociation pathways of gaseous and condensed $Si(CH_3)_2Cl_2$ following Cl 2*p*, Cl 1*s*, and Si 2*p* core-level excitations have been characterized. The excitations to a specific antibonding state ($15a_1^*$ state) of gaseous $Si(CH_3)_2Cl_2$ at the Cl 2*p*, Cl 1*s*, and Si 2*p* edges produce significant enhancement of fragment ions. This ion enhancement at specific core-excited states correlates closely with the ion kinetic energy distribution. The results deduced from ion kinetic energy distribution are consistent with results of quantum-chemical calculations on $Si(CH_3)_2Cl_2$ using the ADF package. The $Cl^-$ desorption yields for $Si(CH_3)_2Cl_2/Si(100)$ at ~90 K are notably enhanced at the $15a_1^*$ resonance at both Cl 2*p* and Si 2*p* edges. The resonant enhancement of $Cl^-$ yield occurs through the formation of highly excited states of the adsorbed molecules. These results provide insight into the state-selective ionic fragmentation of molecules via core-level excitation. © *2006 American Institute of Physics*. [DOI: 10.1063/1.2400229]

## I. INTRODUCTION

The photodissociation of core-excited molecules induced by x-ray photons has received much attention because a comprehensive knowledge of such fragmentation is not only of scientific importance but also of interest in other fields, such as chemical reactions induced by high-energy particles on interstellar dust and radiation damage of biomolecules and x-ray optics. By means of synchrotron radiation with energy tunable in the x-ray region, the site-selective photoexcitation and subsequent cleavage of chemical bonds of molecules on tuning the x-ray energy to a particular absorption resonance have been a subject of extensive research. The site-specific fragmentation via core-level excitation was observed for several systems,[1–9] but not for some molecules.[10,11] A site-specific fragmentation via core-level excitation was observed for several systems,[1–9] but not for some molecules.[10,11] Such photofragmentation of molecules might arise from a rapid dissociation of ions,[12,13] but no direct experimental evidence has been reported. The complicated reaction dynamics involved in site-selective fragmentation of core-excited molecules remains a topic of broad interest.[14–17]

Some highly excited states near or above the threshold energy for double ionization were observed for gaseous samples, such as $SO_2$ and CO,[18–20] but little research has been devoted to these highly excited states and their role on ion desorption processes for adsorbates on surfaces. The detection of negative ions has proved to be a powerful method of exposing highly excited states above the threshold energy for single ionization. However, the investigation of negative-ion fragments produced by inner-shell excitation of molecules is still in its infancy.[18,21–23] The desorption dynamics of negative-ion fragments of absorbates on surfaces following core-level excitation are not yet fully understood.

In this study, the dissociation dynamics for ionic (positive ion and negative ion) fragments from gaseous and condensed $Si(CH_3)_2Cl_2$ following excitations of Cl 2*p*, Cl 1*s*, and Si 2*p* electrons to various resonances have been characterized using synchrotron radiation. The most striking observation is a strong enhancement of fragment ions following excitation of a core electron to a specific unoccupied antibonding valence state ($15a_1^*$ state). We provide a clear demonstration that this ion enhancement of specific core-relaxed states correlates closely with the ion kinetic energy distribution. The $Cl^-$ desorption yields for $Si(CH_3)_2Cl_2/Si(100)$ at ~90 K are enhanced notably at the $15a_1^*$ resonance at both Cl 2*p* and Si 2*p* edges. This resonant enhancement of $Cl^-$ yield occurs through the formation of highly excited states of the adsorbed molecules. These results provide insight into the state-selective enhanced ionic fragments of gaseous and condensed molecules via core-level excitation.

## II. EXPERIMENT

The experimental measurements were conducted at the high-energy spherical grating monochromator (HSGM)

[a)]Authors to whom correspondence should be addressed.
[b)]Electronic mail: jmchen@nsrrc.org.tw

 

beamline and the double-crystal monochromator (DCM) tender x-ray beamline in the National Synchrotron Radiation Research Center (NSRRC) in Taiwan. For dissociation measurements in a condensed phase, an ultrahigh-vacuum (UHV) chamber with a base pressure of $\sim 1 \times 10^{-10}$ Torr was used. The Si(100) surface was cleaned by repeated resistive heating to ~1100 °C under vacuum before the measurements. The high purity $Si(CH_3)_2Cl_2$ (Merck, 99.9%) was degassed by several freeze-pump-thaw cycles before use. The vapor of $Si(CH_3)_2Cl_2$ was then condensed through a leak valve the Si(100) surface at ~90 K. X-ray absorption spectra were recorded by the total-electron yield (TEY) mode using a microchannel plate detector. Negative ions were mass selected with a quadrupole mass spectrometer (Balzers, QMA 410). The quadrupole detector was oriented perpendicular to the substrate surface, and photons were incident at an angle of 45° with respect to the substrate normal. The incident photon intensity ($I_0$) was monitored simultaneously by a Ni mesh located after the exit slit of the monochromator. To measure photodissociation in the gaseous phase, an effusive molecular beam produced by expanding the gas through an orifice (50 $\mu$m) into the experimental chamber was used. The pressure in this chamber was maintained at $\sim 1 \times 10^{-5}$ Torr. Fragment ions were mass selected with a quadrupole mass spectrometer (Hiden, IDP). The ion kinetic energy (not calibrated) was measured by a quadrupole mass spectrometer with a 45° sector field analyzer (Hiden, EQS).

For ion kinetic energy distribution and photodissociation measurements, the HSGM beamline was operated with 100 $\mu$m slits corresponding to the energy resolution of ~0.2 eV at the Cl $2p$ edge and ~0.1 eV at the Si $2p$ edge. To obtain the high-resolution x-ray absorption spectrum, the HSGM beamline was set to a photon resolution of ~0.05 eV at the Si $2p$ edge and ~0.1 eV at the Cl $2p$ edge. The energy resolution of the DCM tender x-ray beamline was set to ~0.6 eV at the Cl $1s$ edge. All yield spectra of fragment ions and x-ray absorption spectra were normalized to the incident photon flux at the Si $2p$, Cl $2p$, and Cl $1s$ edges.

The surface coverage was determined by thermal desorption spectroscopy (TDS). The $Si(CH_3)_2Cl_2$ TDS spectra show a single molecular desorption peak with an exposure of 4 L or less (1 L=$1 \times 10^{-6}$ Torr s). At a higher exposure, additional peak appears at a temperature of ~133 K and its intensity increases with $Si(CH_3)_2Cl_2$ exposures. 4 L exposure of $Si(CH_3)_2Cl_2$ on Si(100) at ~90 K thus corresponds to 1 ML.

## III. RESULTS AND DISCUSSION

Figure 1(a) reproduces the yield spectra of fragment ions from gaseous $Si(CH_3)_2Cl_2$ following Cl $2p$ core-level excitation, with the Cl $L_{23}$-edge x-ray absorption spectrum at the Cl $L_{23}$-edge for comparison. The absorption features labeled as 1, 1′ and 2, 2′ in Fig. 1(a) are ascribed to the transitions to the Cl $2p \rightarrow 15a_1^*$ (Si–Cl) antibonding orbital and Cl $2p \rightarrow 10b_1^*$ (Si–Cl) antibonding orbital, respectively.[24] Excitations to Rydberg orbitals are responsible for the absorption peaks labeled as 3, 3′. The broad band labeled as 4 is attributed to the shape resonance. As shown in Fig. 1(a), the photon-energy dependence of yields of various fragment ions, except $Si(CH_3)_2^+$, $SiCH_3^+$, and $Si^+$, of gaseous $Si(CH_3)_2Cl_2$ resembles the Cl $L_{23}$-edge photoabsorption spectrum. Especially noteworthy is that excitations of Cl $2p$ to the $15a_1^*$ (Si–Cl) antibonding state of gaseous $Si(CH_3)_2Cl_2$ produce significant enhancement of $Si(CH_3)_2^+$ and $SiCH_3^+$ yields.

In Fig. 1(b), the ion yields of various ionic fragments for gaseous $Si(CH_3)_2Cl_2$ as a function of photon energy near the Si $2p$ edge are shown with the gaseous-phase Si $L$-edge x-ray absorption spectrum for comparison. The absorption peaks labeled as 1 and 1′ in Fig. 1(b) are assigned to transitions from $Si(^2P_{3/2,1/2})$ initial states to the $15a_1^*$ (Si–Cl) antibonding orbital. The doublet structures labeled as 2 and 2′ are assigned to excitations to the $17a_1^*$ (Si–Cl) antibonding orbital.[25] This result is consistent with the assignment in the Si $K$-edge absorption spectrum of gaseous-phase $Si(CH_3)_2Cl_2$ by Ferrer *et al.*[26] The higher-energy peak labeled as 5 is due to excitation to Rydebrg orbitals. As noted from Fig. 1(b), the photon-energy dependence of yields of various fragment ions, except $Si(CH_3)_2^+$ and $SiCH_3^+$, of gaseous $Si(CH_3)_2Cl_2$ exhibits a close resemblance to the Si $L_{23}$-edge x-ray absorption spectrum. In contrast, the Si $2p \rightarrow 15a_1^*$ excitation of gaseous $Si(CH_3)_2Cl_2$ induces a substantially enhanced production of $Si(CH_3)_2^+$ and $SiCH_3^+$ yields, particularly of $Si(CH_3)_2^+$.

Figure 2 shows the ion yield spectra of various ionic fragments for gaseous $Si(CH_3)_2Cl_2$ via Cl $1s$ core-level excitation. The Cl $K$-edge x-ray absorption spectrum of gaseous $Si(CH_3)_2Cl_2$ is displayed also in Fig. 2 for comparison. The assignment of the Cl $K$-edge x-ray absorption spectrum of $Si(CH_3)_2Cl_2$ was discussed by Baba *et al.*[27] In contrast to the Cl $K$-edge x-ray absorption spectrum of condensed phase, the double peaks labeled as 1 and 2 are clearly observed in the gaseous-phase $Si(CH_3)_2Cl_2$, as shown in Fig. 2. The absorption peaks labeled as 1 and 2 are virtually ascribed to excitations from Cl $1s$ to the $15a_1^*$ (Si–Cl) and $10b_1^*$ (Si–Cl) antibonding orbitals, respectively, similar to the Cl $L$-edge absorption spectrum. The higher-energy peak labeled as 3 is assigned to be a double excitation.[27]

As noted from Fig. 2, the photon-energy dependence of yields of fragment ions $H^+$, $CH_3^+$, and $Si(CH_3)Cl_2^+$ resembles the Cl $K$-edge x-ray absorption spectrum of gaseous $Si(CH_3)_2Cl_2$. In contrast, a significant dissimilarity of the several ion yield spectra, particularly for $Cl^{2+}$, and the Cl $K$-edge x-ray absorption spectrum of gaseous $Si(CH_3)_2Cl_2$ is observed. As noted, the Cl $1s \rightarrow 15a_1^*$ excitation of gaseous $Si(CH_3)_2Cl_2$ leads to significant enhancement of $Cl^{2+}$ and $SiCH_3^+$ yields, particularly for $Cl^{2+}$. Besides, excitation of Cl $1s$ to a $15a_1^*$ state generates a moderate enhancement of $Cl^+$ and $Si^+$ yields, but a small enhancement of $SiCl^+$ yield. Hence, yields of not only $Cl^+$ and $Cl^{2+}$ but also $Si^+$ and $SiCCH_3^+$ were noticeably enhanced via the Cl $1s \rightarrow 15a_1^*$ excitation of gaseous $Si(CH_3)_2Cl_2$.

Based on the resonant photoemission measurements of gaseous $Si(CH_3)_2Cl_2$, the spectator Auger transitions were the dominant decay channels for resonant excitations of Cl $2p$ (and Si $2p$) to the antibonding valence orbitals ($15a_1^*$ and $10b_1^*$) and Rydberg orbitals of gaseous $Si(CH_3)_2Cl_2$.[7,28] The

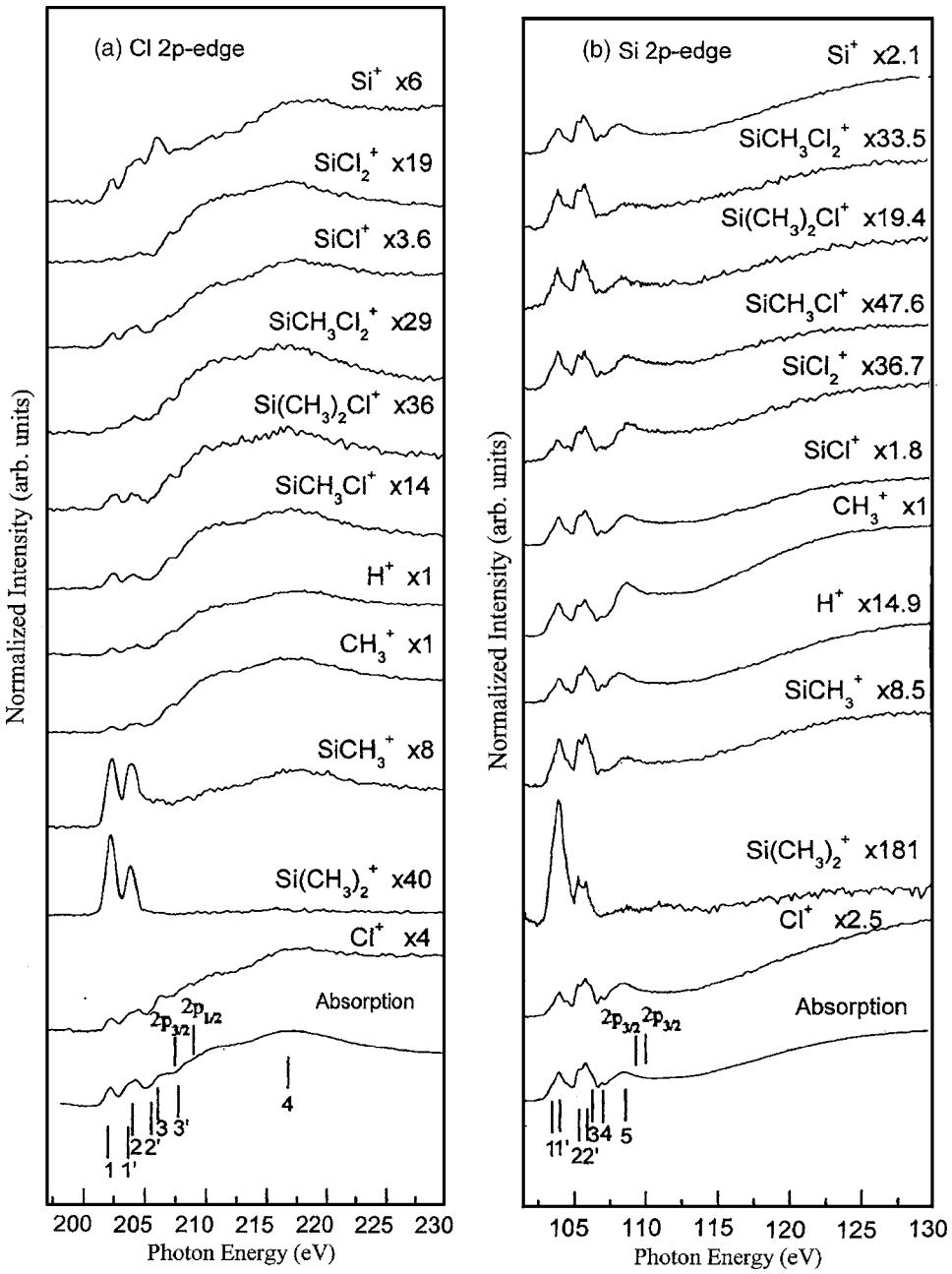


FIG. 1. Photon-energy dependence of fragment ion yields of gaseous $Si(CH_3)_2Cl_2$ following (a) Cl $2p$ and (b) Si $2p$ core-level excitations together with the corresponding photoabsorption spectrum. The ionization thresholds of Cl $2p_{3/2,1/2}$ and Si $2p_{3/2,1/2}$ of gaseous $Si(CH_3)_2Cl_2$ are indicated in the corresponding absorption spectrum.

spectator Auger transition results in a two-hole, one-electron (2h1e) final state, in which two holes are produced in valence orbitals and one electron is excited into an antibonding valence orbital or a Rydberg orbital. The spectator electron is localized at the respective valence orbital during the Auger decay. In contrast, the higher-energy shape resonance excitation is followed by the normal Auger decay, which leads to a two-hole (2h) state. Accordingly, a close resemblance of the fragment ion yield spectra and the corresponding Cl $L$-edge (or Si $L$-edge) x-ray absorption spectra of gaseous $Si(CH_3)_2Cl_2$, as shown in Figs. 1(a) and 1(b), is attributed to the Auger decay of core-excited states and subsequent Coulomb repulsion of multi-valence-hole final states, which was called the Auger-initiated dissociation (AID) mechanism.[29,30]

As shown in Fig. 1(a), the $Si(CH_3)_2^+$ and $SiCH_3^+$ yields show significant enhancement following the Cl $2p \rightarrow 15a_1^*$ excitation when compared with the excitations of Cl $2p \rightarrow 10b_1^*$ and Cl $2p \rightarrow$ shape resonance. This infers that the spectator Auger decay and succeeding 2h1e final states with a spectator electron localized in a strong antibonding orbital $(15a_1^*)$ produce significant enhancement of specific ion fragments. If this hypotheses is correct, it is reasonably expected that these specific 2h1e states populated by spectator Auger transitions of resonant $Si(2p)^{-1}(15a_1^*)^1$ core-excited states of gaseous $Si(CH_3)_2Cl_2$ also lead to strong state-specific ion enhancement. As shown in Fig. 1(b), the yields of $Si(CH_3)_2^+$ and $SiCH_3^+$ via the Si $2p \rightarrow 15a_1^*$ excitation are clearly significantly enhanced, particularly for $Si(CH_3)_2^+$, providing strong evidence to support this hypothesis.

The result deduced from Figs. 1 and 2 clearly reveals that, following the core-to-valence resonance excitation where the spectator Auger decay occurs, the effect of a spectator electron in an antibonding orbital must be taken into account in the ion dissociation processes. As demonstrated, if

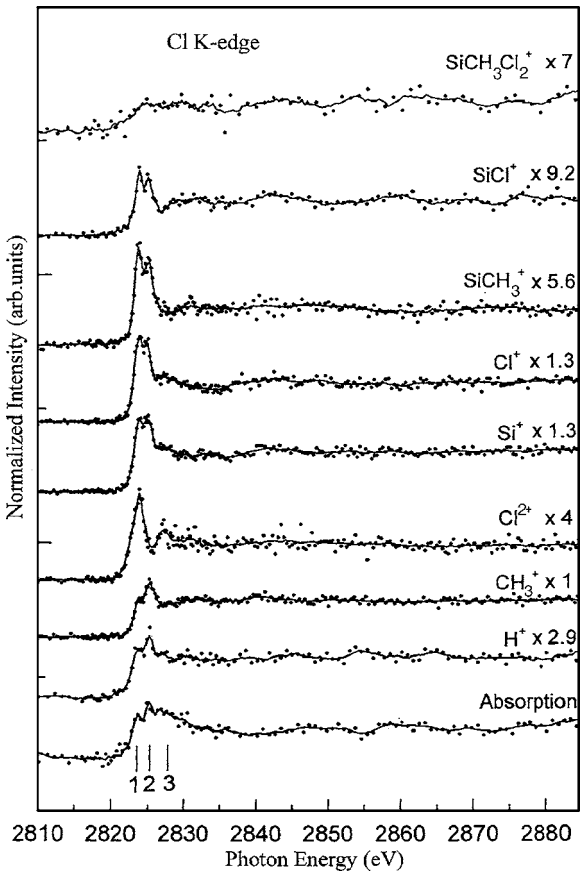


FIG. 2. Photon-energy dependence of fragment ion yields of gaseous $Si(CH_3)_2Cl_2$ near the Cl 1*s* edge with the Cl *K*-edge x-ray absorption spectrum.

the spectator electron is localized in the antibonding orbital with a strong repulsive ionic potential, the breaking of the chemical bond can be enhanced.[31] Hence, the ion yield correlates closely with the slope of repulsive ionic potential. A possible reason for the significant difference in the $Si(CH_3)_2^+$ yields following Cl $2p$ (or Si $2p$) to $15a_1^*$ and $10b_1^*$ excitations might thus reflect the difference in the steepness of the repulsive potential between $15a_1^*$ and $10b_1^*$. It is expected that the potential curve of $15a_1^*$ is much steeper than that of $10b_1^*$. So, within the lifetime of 2h1e, $Si(CH_3)_2^+$ can gain more kinetic energy from $15a_1^*$ state, increasing the $Si(CH_3)_2^+$ yield.

The kinetic energy distribution of ionic fragments produced by photoexcitation of molecules provides information about the dissociation dynamics such as the steepness of potential energy surfaces of electronically relaxed states and the energy partitioning among the internal degree of freedom of fragments.[32] To elucidate the mechanism of state-specific enhancement of ionic fragments, we measure the kinetic energy distributions of various fragment ions from gaseous $Si(CH_3)_2Cl_2$ following Cl $2p$ and Si $2p$ core-level excitations to various resonances. In Figs. 3(a)–3(c), the average kinetic energies of fragment ions [$SiCl^+$, $Si^+$, and $Si(CH_3)_2Cl^+$, as representative examples] are shown as a function of the excitation energy near the Cl $2p$ edge. As noted, the average kinetic energies of fragment ions depend markedly on the excitation energy.

As shown in Figs. 3(a)–3(c), the average kinetic energies of various fragment ions, such as $SiCl^+$, at the shape resonance are much higher than those at Cl $2p$ core-to-valence and Cl $2p$ core-to-Rydberg excitations. This is due to the fact that the Coubomb repulsion of electronically relaxed two-hole (2h) states at the shape resonance is much larger than that of 2h1e final states at resonant Cl $2p$ core-to-valence and Cl $2p$ core-to-Rydberg excitations. In Fig. 3(d), the kinetic energy distributions of $Si(CH_3)_2^+$ from gaseous $Si(CH_3)_2Cl_2$ following Cl $2p$ core-level excitation are reproduced. The resultant average kinetic energy of $Si(CH_3)_2^+$ is shown in Fig. 3(e) as a function of the excitation energy near the Cl $2p$ edge. As noted from Figs. 3(d) and 3(e), the ion kinetic energy distribution of $Si(CH_3)_2^+$ via the Cl $2p \rightarrow 15a_1^*$ excitation is shifted to an energy of ~0.2–0.3 eV greater than those via excitations of Cl $2p$ to $10b_1^*$, state, Rydberg orbital, and shape resonance. As mentioned, the kinetic-energy distribution of ionic fragments from molecules via core-level excitation is related to the steepness of the potential energy curves of the electronically relaxed states.[32] Accordingly, the electronically relaxed $2h(15a_1^*)^1$ states with a spectator electron localized at the $15a_1^*$ states would have steeper repulsive-potential curves along the Si–Cl coordinates than for $2h(10b_1^*)^1$ and 2h states.

After spectator Auger decay of resonant core-excited molecules, the kinetic energy released to the dissociation processes is given the difference between the Coulomb repulsive energy of two holes and the dissociation energy of a specific bonding. We assumed that the Coulomb repulsive energy of two holes produced by the $Cl(2p)^{-1}15a_1^*$ resonance is approximately the same as that generated by the $Cl(2p)^{-1}10b_1^*$ resonance. As presented in Fig. 3, the kinetic energy for ionic fragment $Si(CH_3)_2^+$ via the Cl $2p \rightarrow 15a_1^*$ excitation of gaseous $Si(CH_3)_2Cl_2$ is ~0.2–0.3 eV greater than that via the Cl $2p \rightarrow 10b_1^*$ excitation. Hence the dissociation energy of Si–Cl bonding of $Si(CH_3)_2Cl_2$ at the 2h1e states with a spectator electron in the $15a_1^*$ orbital is smaller than that at the 2hle states with a spectator electron in the $10b_1^*$ orbital.

Based on the molecular-orbital calculations in $Si(CH_3)_2Cl_2$ performed with the ADF package, the atomic populations of the Si–Cl orbital, such as $11a_1$ state, are composed mainly of Si $3s$ orbital and Cl $3p$ orbital. It is therefore expected that the spectator electron in the Si $3s^*$ orbital or Cl $3p^*$ orbital assists in breaking the Si–Cl bond. The $15a_1^*$ orbital is composed of Si $3s$ (22%), Si $3p$ (34%), Cl $3p$ (26%), and other minor components. The $10b_1^*$ orbital consists mainly of Si $3s$ (<1%), Si $3p$ (61%), and Cl $3p$ (10%). The contents of the Si $3s^*$ and Cl $3p^*$ orbital components in the $15a_1^*$ orbital are much greater than those in the $10b_1^*$ orbital. As a result, a spectator electron in the $15a_1^*$ orbital is more effective in the cleavage of the Si–Cl bond than that in the $10b_1^*$ orbital. This theoretical prediction is consistent with the present ion kinetic energy distribution measurements.

Figures 4(a) and 4(b) show the average kinetic energies of $SiCl^+$ and $Cl^+$ ions, respectively, as a function of the excitation energy in the vicinity of Si $2p$ edge. Similar to the Cl $2p$ edge, the average kinetic energies of $SiCl^+$ and $Cl^+$ ions above the Si $2p$ ionization threshold (~109.3 eV for Si $2p_{3/2}$

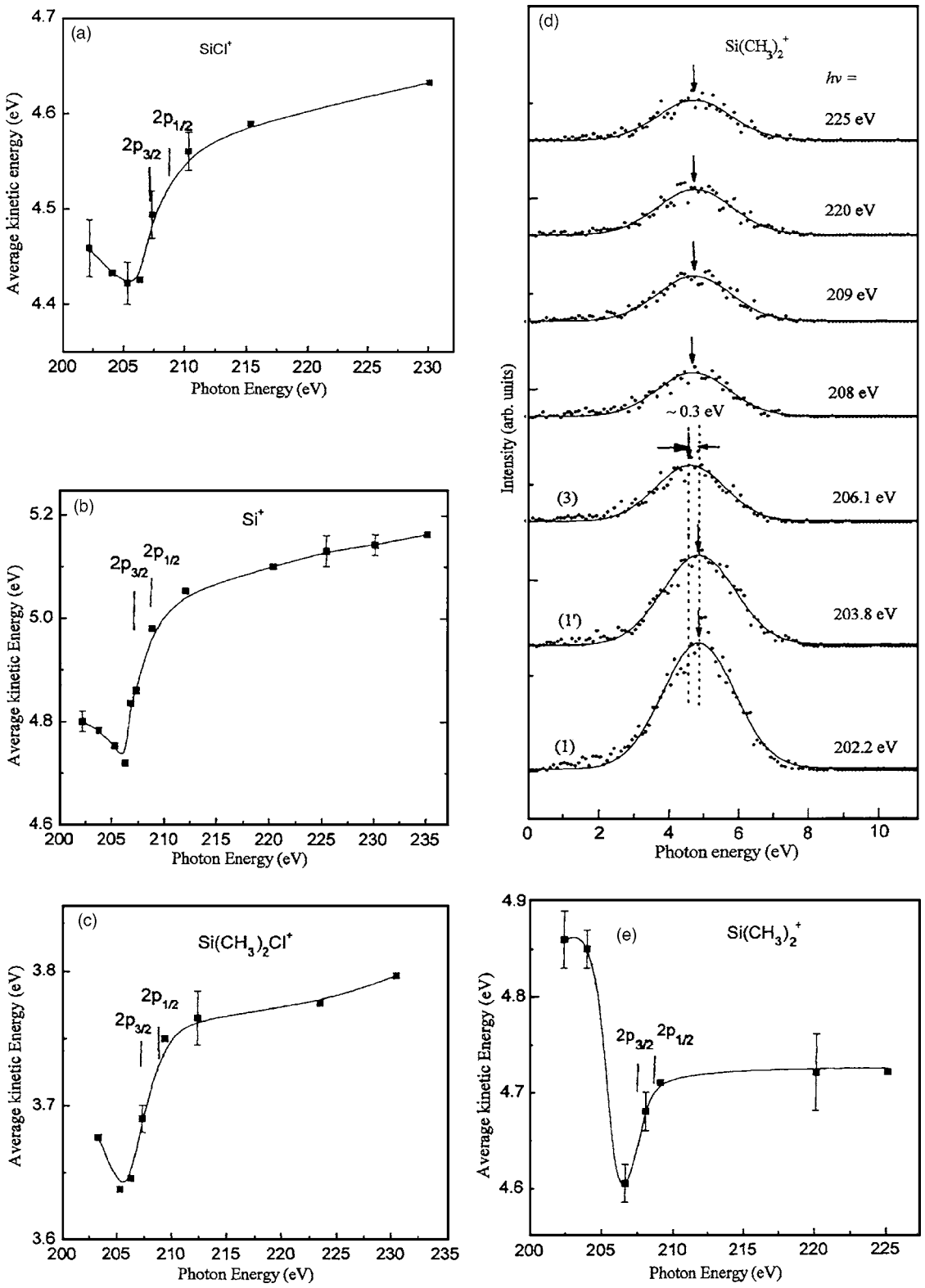


FIG. 3. Average kinetic energies of (a) $SiCl^+$, (b) $Si^+$, and (b) $Si(CH_3)_2Cl^+$ as a function of excitation energy near the Cl $2p$ edge. (d)Kinetic energy distributions of $Si(CH_3)_2^+$ of gaseous $Si(CH_3)_2Cl_2$ following Cl $2p$ core-level excitation. The photon energy used for excitation is indicated in each spectrum. The number indicated in each spectrum corresponds to an absorption peak marked in the absorption spectrum in Fig. 1(a). (e)Average kinetic energy of $Si(CH_3)_2^+$ as a function of the photon energy in the vicinity of the Cl $2p$ edge.

ionization threshold) exceed those at Si $2p$ core-to-valence excitations. In Fig. 4(c), the ion kinetic energy distributions of $Si(CH_3)_2^+$ of gaseous $Si(CH_3)_2Cl_2$ following Si $2p$ core-level excitation are reproduced. The resultant average kinetic energy of $Si(CH_3)_2^+$ is shown Fig. 4(d) as a function of the excitation energy in the vicinity of the Si $2p$ edge. As noted from Figs. 4(c) and 4(d), the average kinetic energy for fragment $Si(CH_3)_2^+$ at the $Si(2p)^{-1}(15a_1^*)^1$ resonance is greater than those at the $Si(2p)^{-1}(17a_1^*)^1$ resonance and above the Si $2p$ ionization threshold. Hence the slope of the potential en-

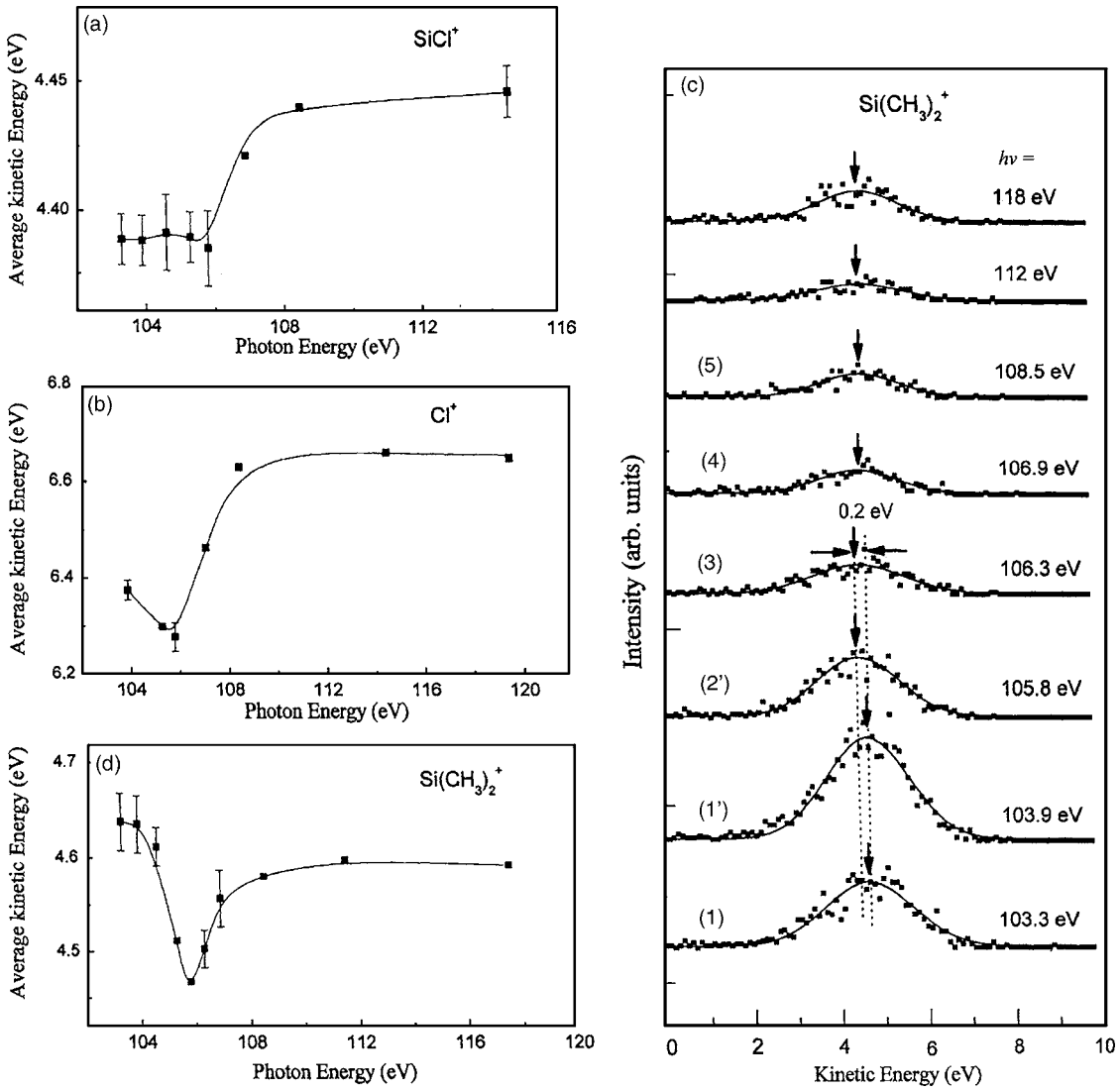


FIG. 4. Average kinetic energies of (a) $SiCl^+$ and (b) $Cl^+$ as a function of excitation energy near the Si $2p$ edge. (d) Kinetic energy distributions of $Si(CH_3)_2^+$ of gaseous $Si(CH_3)_2Cl_2$ following Si $2p$ core-level excitation. The photon energy used for excitation is indicated in each spectrum. The number indicated in each spectrum corresponds to an absorption peak marked in the absorption spectrum in Fig. 1(b). (e) Average kinetic energy of $Si(CH_3)_2^+$ as a function of the photon energy in the vicinity of the Si $2p$ edge.

ergy curves along the Si–Cl coordinates of the electronically relaxed $2h(15a_1^*)^1$ states is steeper than those of the $2h(17a_1^*)^1$ and 2h states, as confirmed by Cl $2p$ excitation in Figs. 3(d) and 3(e). The enhancement of the $Si(CH_3)_2^+$ yield at the specific resonance therefore correlates strongly with the ion kinetic energy distribution which is related to the steepness of potential surface of core-relaxed states. Accordingly, after spectator Auger decay of resonant Si $2p$, Cl $2p$, and Cl $1s$ core-excited states of gaseous $Si(CH_3)_2Cl_2$, the subsequent electronically relaxed 2h1e or multihole, one-electron (mh1e) final states with a steeper potential energy surface along the dissociation coordinates lead to significant enhancement of specific ion fragments. The present results clearly demonstrate that the bond breaking is assisted by a specific antibonding state, not just any antibonding state. Perhaps for this reason site selectivity was not found in some molecules.[11]

Unlike positive-ion desorption, $Cl^-$ and $H^-$ were the ions predominantly observed in the negative-ion desorption of $Si(CH_3)_2Cl_2/Si(100)$ following Cl $2p$ and Si $2p$ core-level excitations. Figures 5(a) and 5(b) show the $Cl^-$ yield and $H^-$ yield spectra from $Si(CH_3)_2Cl_2/Si(100)$ following Cl $2p$ and Si $2p$ core-level excitations, respectively, with the corresponding Cl $L$-edge and Si $L$-edge TEY spectra of condensed $Si(CH_3)_2Cl_2$ for comparison. As noted from Figs. 5(a) and 5(b), the $H^-$ yield curves nearly follow the corresponding Cl $L$-edge and Si $L$-edge total electron yield curves. The possible desorption mechanism of $H^-$ from $Si(CH_3)_2Cl_2/Si(100)$ was likely due to dissociative attachment on molecules of secondary electrons produced by photoabsorption of molecular adsorbates. This desorption mechanism was called dissociative electron attachment (DEA). Also, the $H^-$ and $Cl^-$ yields at ~101 eV, indicated by arrows in Fig. 5(b), are induced by the secondary electrons produced by the Si $2p$ core-level excitation of the Si(100) substrate, likewise providing evidence of the existence of DEA processes.[22,33]

Especially noteworthy is that the Cl $2p \rightarrow 15a_1^*$ excitation

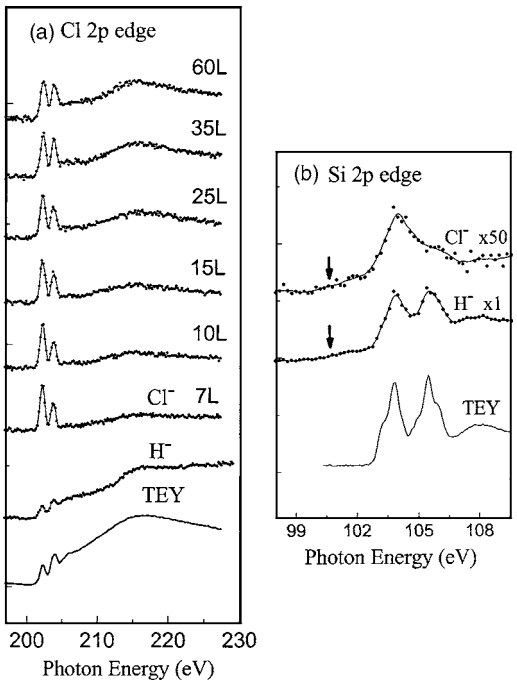


FIG. 5. (a) $H^-$ yield and $Cl^-$ yield spectra for $Si(CH_3)_2Cl_2/Si(100)$ at ~90 K in the vicinity of (a) the Cl $2p$ edge and (b) the Si $2p$ edge along with the corresponding Cl $L$-edge and Si $L$-edge TEY spectra for comparison.

significantly enhanced the $Cl^-$ desorption yield. To elucidate the origin of the $Cl^-$ enhancement at the $15a_1^*$ resonance, we measured the $Cl^-$ yield spectra from $Si(CH_3)_2Cl_2/Si(100)$ with variable coverage following Cl $2p$ core-level excitation, as presented in Fig. 5(a). As noted, the $Cl^-$ yield at shape resonance increases with $Si(CH_3)_2Cl_2$ exposures and thus show a linear behavior with electron yield. Hence the desorption mechanism of $Cl^-$ at shape resonance excitation for $Si(CH_3)_2Cl_2/Si(100)$ is likely due to DEA. If the enhancement of $Cl^-$ yield at the $15a_1^*$ resonances is due to a DEA process, the $Cl^-$ yield at the $15a_1^*$ resonance should show a trend like that at the shape resonance, because the energy distribution of the secondary electrons becomes indistinguishable for photoexcitation at shape resonance and at other photon energies. Hence, the $Cl^-$ yield at the $15a_1^*$ resonance should monotonically increase with $Si(CH_3)_2Cl_2$ exposure. However, as noted from Fig. 5(a), the $Cl^-$ yield at the $15a_1^*$ resonance increased up to 10 L exposure and then slowly decreased after 10 L exposure of $Si(CH_3)_2Cl_2$ on Si(100). Moreover the observed $15a_1^*$ resonances have the same energies and widths between $Cl^-$ yield and TEY spectra. It allows us to give a reasonable explanation that the enhancement of $Cl^-$ yield at the $15a_1^*$ resonance is due not to DEA processes but to unimolecular processes.

It is speculated that the enhancement of $Cl^-$ yield at the $Cl(2p)^{-1}15a_1^*$ resonance might originate from some highly excited states of the parent ions that are predissociated by an ion-pair or direct dissociation.[18–20] It was proposed that the core-excited states of $Si(CH_3)_2Cl_2$ molecules via the Cl $2p$ core-level excitation can decay by an Auger transition to these highly excited states. If such highly excited states exist, it is thus expected that these states can also be populated by an Auger transition of Si $2p$ core-excited states of $Si(CH_3)_2Cl_2$. As shown in Fig. 5(b), the $Cl^-$ yield at ~103.8 eV via the Si $2p \rightarrow 15a_1^*$ excitation shows a notable enhancement relative to that at ~105.5 eV on excitation to Si–C antibonding states. This gives evidence in support of the existence of some highly excited states. A similar phenomenon has been found for $OPCl_3$ (P $2p$ and Cl $2p$ edges), $Si(CH_3)_{4-n}Cl_n$ ($n=1-4$) (Si $2p$ and Cl $2p$ edges), etc.[21] The formation of negative ions through highly excited states is thus not specific to $Si(CH_3)_2Cl_2$ molecules. It is therefore believed that the present experimental finding is of a general nature.

## IV. CONCLUSION

In conclusion, the state-selective positive-ion and negative-ion dissociation pathways of gaseous and condensed $Si(CH_3)_2Cl_2$ following Cl $2p$, Cl $1s$, and Si $2p$ core-level excitations have been characterized using photon-induced dissociation, x-ray absorption spectroscopy, and ion kinetic energy distribution. The excitations to a specific antibonding state ($15a_1^*$ state) of gaseous $Si(CH_3)_2Cl_2$ at the Cl $2p$, Cl $1s$, and Si $2p$ edges lead to significant enhancement of fragment ions. This ion enhancement at specific core-excited states correlates strongly with the ion kinetic energy which is related to the steepness of a potential surface along the dissociation coordinates of core-relaxed states. The results deduced from ion kinetic energy distribution are consistent with results of molecular orbital calculations on $Si(CH_3)_2Cl_2$ using the ADF package. The $Cl^-$ desorption yields from $Si(CH_3)_2Cl_2/Si(100)$ at ~90 K are notably enhanced at the $15a_1^*$ resonance at both Cl $2p$ and Si $2p$ edges. The resonant enhancement of $Cl^-$ yield occurs through the formation of highly excited states of the adsorbed molecules. These highly excited states hence play an important role in ion desorption of adsorbed molecules via core-level excitation. Our experimental results provide important insight into the roles and relative importance of dissociative electron attachment, highly excited states, and Auger initiated desorption. These results contribute to a comprehensive understanding of the state-selective ionic (positive ions and negative ions) fragmentation of gaseous and condensed molecules via core-level excitation.

## ACKNOWLEDGMENTS

We thank the NSRRC staff for their technical support. This research is supported by the NSRRC and the National Science Council of the Republic of China under Grant No. NSC 94-2113-M-213-001 and NSC 93-2113-M-213-009.

[1] W. Eberhardt, T. K. Sham, R. Carr, S. Krummacher, M. Strongin, S. L. Weng, and D. Wesner, Phys. Rev. Lett. **50**, 1038 (1983).
[2] X. J. Liu, G. Prümper, E. Kukk *et al.*, Phys. Rev. A **72**, 042704 (2005).
[3] R. Romberg, N. Heckmair, S. P. Frigo, A. Ogurtsov, D. Menzel, and P. Feulner, Phys. Rev. Lett. **84**, 374 (2000).
[4] Y. Baba, K. Yoshii, and T. A. Sasaki, J. Chem. Phys. **105**, 8858 (1996).
[5] S. Nagaoka, K. Mase, M. Nagasono, S. Tanaka, T. Urisu, and J. Ohshita, J. Chem. Phys. **107**, 10751 (1997).
[6] M. C. K. Tinone, K. Tanaka, J. Maruyama, N. Ueno, M. Imamura, and N. Matsubayashi, J. Chem. Phys. **100**, 5988 (1994).

[7] J. M. Chen, K. T. Lu, J. M. Lee, C. I. Ma, and Y. Y. Lee, Phys. Rev. Lett. **92**, 243002 (2004).
[8] S. I. Nagaoka, K. Mase, and I. Kayano, Trends Chem. Phys. **6**, 1 (1997).
[9] N. Saito, J. D. Bozek, and I. H. Suzuki, Chem. Phys. **188**, 367 (1994).
[10] I. Nenner and P. Morin, in *VUV and Soft X-Ray Photoionization*, edited by U. Becker and D. A. Shirley (Plenum, New York, 1996).
[11] M. Simon, T. Lebrun, R. Martins, G. G. B. De Souza, I. Nenner, M. Lavollee, and P. Morin, J. Phys. Chem. **97**, 5228 (1993).
[12] Y. Baba, K. Yoshii, and T. A. Sasaki, Surf. Sci. **357–358**, 302 (1996).
[13] R. Thissen, W. Simon, and M. J. Hubin-Franskin, J. Chem. Phys. **101**, 7548 (1994).
[14] Y. Baba, Low Temp. Phys. **29**, 228 (2003), and references therein.
[15] S. Svensson, J. Phys. B **38**, S821 (2005), and references therein.
[16] K. Ueda, J. Phys. B **36**, R1 (2003), and references therein.
[17] K. Ueda and J. H. D. Eland, J. Phys. B **38**, S839 (2005).
[18] G. Dujardin, L. Hellner, B. J. Olsson, M. J. Besnard-Ramage, and A. Dadouch, Phys. Rev. Lett. **62**, 745 (1989).
[19] W. C. Stolte, D. L. Hansen, M. N. Piancastelli, I. Dominguez Lopez, A. Rizvi, O. Hemmers, H. Wang, A. S. Schlachter, M. S. Lubell, and D. W. Lindle, Phys. Rev. Lett. **86**, 4504 (2001).
[20] A. Dadouch, G. Dujardin, L. Hellner, M. J. Besnard-Ramage, and B. J. Olsson, Phys. Rev. A **43**, 6057 (1991).
[21] J. M. Chen and K. T. Lu, Phys. Rev. Lett. **86**, 3176 (2001).
[22] P. Roncin, A. G. Borisov, H. Khemliche, A. Momeni, A. Mertens, and H. Winter, Phys. Rev. Lett. **89**, 043201 (2002).
[23] S. W. J. Scully, R. A. Mackie, R. Browning, K. F. Dunn, and C. J. Latimer, Phys. Rev. A **70**, 042707 (2004).
[24] J. M. Chen, K. T. Lu, R. G. Liu, J. W. Lay, Y. C. Liu, and T. J. Chuang, J. Chem. Phys. **108**, 7849 (1998).
[25] J. M. Chen, K. T. Lu, R. G. Liu, J. M. Lay, and Y. C. Liu, J. Chem. Phys. **106**, 9105 (1997).
[26] J. L. Ferrer, S. Bodeur, and I. Nenner, J. Electron Spectrosc. Relat. Phenom. **52**, 711 (1990).
[27] Y. Baba, K. Yoshii, H. Yamamoto, and T. A. Sasaki, J. Phys.: Condens. Matter **7**, 1991 (1995).
[28] J. M. Chen, K. T. Lu, J. M. Lee, S. C. Ho, H. W. Chang, and Y. Y. Lee, J. Electron Spectrosc. Relat. Phenom. **144–147**, 171 (2005).
[29] L. Knotek and P. J. Feibelman, Phys. Rev. Lett. **40**, 964 (1978).
[30] P. J. Feibelman, Surf. Sci. **102**, L51 (1981).
[31] J. M. Chen, K. T. Lu, and J. M. Lee, J. Chem. Phys. **118**, 5087 (2003).
[32] R. Weimar, R. Romberg, S. F. Frigo, B. Kassühlke, and P. Feulner, Surf. Sci. **451**, 124 (2000).
[33] L. G. Christophorou, D. L. McCorkle, and A. A. Christodoulides, in *Electron-Molecule Interactions and Their Applications*, edited by L. G. Christophorou (Academic, Orlando, 1984), Vol. 1.